



The critical role of oxygenated volatile organic compounds (OVOCs) in shaping photochemical O₃ chemistry and control strategy in a subtropical coastal environment

Lirong Hui¹, Yi Chen^{1,2}, Xin Feng¹, Hao Sun¹, Jia Guo³, Yang Xu¹, Yao Chen¹, Penggang
5 Zheng¹, Dasa Gu¹ and Zhe Wang^{1,*}

¹ Division of Environment and Sustainability, The Hong Kong University of Science and Technology, Hong Kong SAR, 999077, China

² Department of Chemistry, The Hong Kong University of Science and Technology, Hong Kong SAR, China

10 ³ Environmental Central Facility, Institute of Environment, The Hong Kong University of Science and Technology, Hong Kong SAR, 999077, China

*Correspondence to: Zhe Wang: z.wang@ust.hk

15 Abstract

Photochemical ozone (O₃) pollution remains a persistent environmental challenge, and growing evidence highlights the critical role of oxygenated volatile organic compounds (OVOCs) in photochemical processes. However, comprehensive and quantitative measurements of OVOCs remain limited. This study investigates the impact of OVOCs on O₃
20 formation mechanisms and radical budgets by integrating high-resolution field measurements from a subtropical coastal region in South China with observation-based photochemical modeling. 63 OVOC species were quantified by a proton-transfer-reaction time-of-flight mass spectrometry (PTR-ToF-MS), and account for 72%-77% of total VOC concentrations. The O₃-precursor relationship analysis revealed a transition regime for O₃ formation and high sensitivity
25 to OVOCs. OVOC-related reactions, including OVOC photolysis, OVOC oxidation by OH and NO₃ radicals, contributed approximately 36%-73% to daytime production rates of HO₂ and RO₂ radicals. Model simulations without comprehensive consideration of OVOCs would significantly underestimate daytime production rates of O₃ and RO_x radicals by 41%-48%, and shift the diagnosis of O₃ formation from a transition regime to a VOC-limited regime, leading
30 to biased policy recommendations and potentially ineffective control strategies. These findings underscore the critical role of OVOCs in atmospheric photochemistry and highlight the urgent need for comprehensive OVOC quantification to improve OVOC-inclusive model frameworks.



Such improvements are essential for accurately characterizing O₃-precursor relationships and for developing effective and sustainable strategies to mitigate regional O₃ pollution.

35 1. Introduction

Ground-level ozone (O₃) is a significant secondary air pollutant and a major component of photochemical smog, posing serious threats to human health, ecosystems, and the climate (Feng et al., 2019; Yue and Unger, 2014; Mills et al., 2018). Elevated O₃ levels remain a persistent environmental challenge in many urban regions worldwide, especially a notable
40 upward trend in East Asia (Li et al., 2019b; Li et al., 2020). O₃ formation in the troposphere arises from complex photochemical reactions involving nitrogen oxides (NO_x) and volatile organic compounds (VOCs) under the sunlight (Zhao et al., 2022; Xu et al., 2022). The oxidation of VOCs by hydroxyl (OH) radical plays a central role in producing peroxy radicals, such as hydroperoxyl (HO₂) and alkyl peroxy (RO₂) radicals, which sustain the chain reactions
45 driving photochemical O₃ production (Lyu et al., 2022).

Previous studies have underscored the importance of non-methane hydrocarbons, particularly alkenes and aromatics, as major precursors of O₃ formation, leading to targeted control measures in various regions (Li et al., 2015; Li et al., 2017; Hong et al., 2019). However, recent research highlights the crucial roles of oxygenated VOCs (OVOCs) in regulating
50 atmospheric oxidation capacity and contributing to radical production (Wang et al., 2022a; Shen et al., 2021; Chai et al., 2023; Yang et al., 2023). OVOCs, such as carbonyls and alcohols, can be emitted directly from diverse sources or formed as secondary products from VOC oxidation (Mellouki et al., 2003). These OVOC compounds can further react with OH radical or undergo photolysis processes, serving as significant sources of HO₂ and RO₂ radicals that
55 amplify radical cycling and promote O₃ formation (Xue et al., 2016; Chen et al., 2020; Huang et al., 2020b). Despite their importance, the diversity and high reactivity of OVOCs introduce substantial uncertainties in atmospheric chemistry and air quality models, particularly in regions with limited OVOC measurements.

Traditional analytical techniques such as gas chromatography (GC) coupled with flame
60 ionization or mass spectrometry detection (FID/MS) have been widely used to measure non-methane hydrocarbons, but only a subset of OVOCs (Huang et al., 2015; Yang et al., 2019; Li et al., 2019a; Han et al., 2019). High-performance liquid chromatography (HPLC) can detect several carbonyl compounds, such as formaldehyde, acetaldehyde, acetone, but its reliance on offline sampling limits its temporal resolution, making it less effective for capturing real-time
65 atmospheric variations (Lu et al., 2010; Yang et al., 2017; Zhang et al., 2024). Furthermore,



many other key OVOC species, such as larger aldehydes, ketones, carboxylic acids, organic peroxides, and other multifunctional compounds, have been rarely measured and poorly characterized in ambient air, which may result in underestimating the role of OVOCs in atmospheric chemistry (Wang et al., 2022a). While NO_x and VOCs are well-recognized as the primary drivers of O₃ formation, the role of OVOCs in shaping photochemical O₃ chemistry has received comparatively less attention due to limited field observations and insufficient representation in chemical models. In addition, previous model studies tended to considerably underestimate RO_x (OH, HO₂ and RO₂) radicals compared to observation (Hofzumahaus et al., 2009; Ma et al., 2019; Rohrer et al., 2014). Some studies have attempted to address these gaps by simulating unmeasured OVOC species using photochemical box model, but large uncertainties still exist, largely due to missing OVOC primary sources, incomplete or underestimated secondary chemical pathways (Karl et al., 2018; Mo et al., 2016; Bloss et al., 2005; Li et al., 2014). These knowledge gaps hinder an accurate understanding of the O₃-precursor relationship, complicating the development of effective control strategies.

To gain a comprehensive understanding of the role of OVOCs in photochemical O₃ chemistry, a continuous field campaign was conducted at a coastal suburban site in Hong Kong in South China. High-resolution measurements of more than sixty OVOC species were measured using proton-transfer-reaction time-of-flight mass spectrometry (PTR-ToF-MS). By integrating these measurements into a model simulation framework, we quantified the contributions of OVOCs to radical production and O₃ formation, and examined their impacts on O₃-precursor relationship, providing critical insights into the formulation of targeted strategies for mitigating O₃ pollution in this subtropical region and similar environments.

2. Methodology

2.1 Field measurement and instrumentation

Field measurements were conducted at a suburban coastal site (22.33°N, 114.27°E) located at the campus of The Hong Kong University of Science and Technology (HKUST) in eastern Hong Kong. Situated on a cliff overlooking the sea, the site is near a hotel and a construction project, which may introduce influences from construction activities, household activities, and vehicle emissions. The continuous field campaign spanned from September 4 to December 20 in 2021, covering three seasons: summer (September 4 - October 12), autumn (October 13 - December 1), and early winter (December 2 - December 20). Seasonal divisions was based on the timing of the first synoptic event, as detailed in our previous studies (Feng et



al., 2023). The measurement site is generally affected by long-range regional transport of aged air masses from South and East China due to the Asian monsoon, as well as fresh emission plumes from Hong Kong and the Pearl River Delta region (Ding et al., 2013).

A PTR-ToF-MS (Ionicon Analytik GmbH, Innsbruck, Austria) with H_3O^+ as the primary reaction ion was used to measure the gaseous VOC and OVOC species. Ambient air was drawn into the sampling manifold via a 1/16 polyetheretherketone (PEEK) tube at a flow rate of 5 L min^{-1} , and a subsample of filtered air (100 mL min^{-1}) was directed to the PTR-ToF-MS inlet, protected by a polytetrafluoroethylene (PTFE) membrane particle filter to exclude dust and debris. The sampling inlet was maintained at 80°C throughout the measurements to mitigate humidity-related effects, reduce adsorption losses, and ensure gas-phase stability of target compounds prior to entering the drift tube. The instrument operated under optimized conditions: drift tube temperature maintained at 80°C , drift voltage at 520 V, and drift tube pressure at 2.8 mbar, achieving a field density ratio (E/N) of 98 Td ($1 \text{ Td} = 10^{-17} \text{ V cm}^2$). A relatively higher E/N ratio was employed to suppress the formation of water clusters, thereby minimizing the strong humidity dependence of the target species (Yuan et al., 2017).

Automatic mass calibration was conducted every 100 seconds using the built-in Ionicon permeation unit (PerMasCal), which releases strong signals of m/z 203.943 ($\text{C}_6\text{H}_4\text{I}_2\text{H}^+$, fragment) and m/z 330.848 ($\text{C}_6\text{H}_4\text{I}_2\text{H}^+$). Background measurement and multi-point calibration were conducted periodically during the field campaign using a Liquid Calibration Unit (LCU, Ionicon) with pure nitrogen and multi-component VOC gas standards. 19 VOC/OVOC standard gases were used for multi-point calibration, achieving linear correlation coefficients (R^2) above 0.99 (Table S1). The limit of detection (LOD) for each species was defined as three times the standard deviation (3σ) of background signal (Zhou et al., 2019), ranged from approximately 0.009 to 0.094 ppbv (Table S1). Transmission correction was applied using a set of reference compounds, including benzene (m/z 79.054), toluene (m/z 93.070), m-xylene (m/z 107.086), 1,2,4-trimethylbenzene (m/z 121.101), dichlorobenzene (m/z 146.976), and trichlorobenzene (m/z 180.937). In total, 117 VOC/OVOC species were identified and quantified by attributing the measured ion masses to the most plausible molecular contributors, based on established references and prior studies (Yuan et al., 2017; Koss et al., 2018; Wu et al., 2020), as summarized in Table S2. For species lacking calibration standards, concentrations were determined using an assumed proton transfer reaction rate coefficient of $2 \times 10^{-9} \text{ cm}^3 \text{ s}^{-1}$, combined with mass-dependent transmission correction (Zhang et al., 2022).

However, we acknowledge the several caveats associated with the VOC/OVOC quantification. First, PTR-ToF-MS is limited in its ability to differentiate between isomeric



compounds. Most molecular formulas were therefore evenly distributed among potential isomers (e.g., phenols, nitrophenols), while specific formulas for aldehydes and ketones were identified based on prior studies using GC-PTR-ToF measurement (Koss et al., 2018).

135 Although we attempted to assign signals based on likely contributors informed by literature, this approach introduces uncertainties in the molecular-level identification. Second, the ions detected by PTR-ToF-MS can include fragmentation products or hydrated clusters, particularly for highly functionalized OVOCs, which may lead to over- or underestimation of specific compounds if not correctly interpreted. These effects are especially relevant for larger or
140 multifunctional OVOCs that are more prone to fragmentation or clustering. Given these limitations, our quantification of OVOCs should be considered semi-quantitative for uncalibrated species.

In addition, daytime canister samples of VOCs were collected daily in three seasons, and nonmethane hydrocarbons and alkyl nitrates were analyzed using gas chromatograph
145 system equipped with mass spectrometry, flame ionization, and electron capture detectors (GC-MS/FID/ECD). Trace gases including O₃, NO_x (nitric oxide (NO) and nitrogen dioxide (NO₂)) and carbon monoxide (CO) were measured by O₃ analyzer (Thermo Scientific, model 49i), NO_x analyzer (Ecotech Serinus 40) and CO analyzer (Thermo Scientific, model T300), respectively. The meteorological parameters including temperature (T), relative humidity (RH),
150 wind speed (WS), and wind direction (WD) were recorded by a Weather Station. Detailed descriptions of the instruments are available in previous work (Hui et al., 2023; Sun et al., 2024).

2.2 Photochemistry Modeling

A zero-dimensional photochemical box model (the Framework for 0-D Atmospheric
155 Modeling, F0AM v4.2.2) coupled with the Master Chemical Mechanism (MCM) v3.3.1 was applied to simulate the atmospheric photochemistry of observed species. The MCM v3.3.1 is a nearly explicit gas-phase chemical mechanism describing over 17000 reactions and 5800 primary, secondary, and radical species. The model simulation was constrained by observed hourly data of meteorological parameters (T, RH, and pressure), trace gases (O₃, NO, NO₂, and
160 CO), 38 VOC species measured by GC-MS/FID/ECD (Table S3), and 88 VOC/OVOC species measured by PTR-ToF-MS (Table S2). VOC species from daytime canister samples were linearly interpolated to hourly resolution for the model input (Yang et al., 2018), while nighttime data were approximated using linear regressions of unmeasured concentrations of C₂-C₁₀ hydrocarbons and alkyl nitrates against continuous measured hydrocarbons (e.g., C₃H₆,



165 C₅H₁₀, C₆H₁₀) and nitrophenols by PTR-ToF-MS, respectively. These approximations were used primarily to pre-run the model and were not expected to affect daytime simulation results (Chen et al., 2020). Photolysis frequencies within the model were calculated as the function of solar zenith angle (Wolfe et al., 2016). Observation-based simulations were performed for consecutive days with high O₃ concentrations during summer (September 8 - October 2),
170 autumn (November 12 - November 30), and early winter (December 4 - December 19). Three days from summer (September 11, 12, and 17) were selected as the case study of summer high-O₃ episode, where the maximum O₃ concentration exceeded 110 ppbv. The model was pre-run for four days to stabilize the concentrations of unconstrained species, with results from the 5th day used for further analysis.

175 Model performance was evaluated using the index of agreement (IOA), as illustrated in Equation 1 (Huang et al., 2005), with values of 0.81-0.87 for the simulated O₃ across seasons in this study, comparable to previous studies (0.6-0.9), suggesting that the abundance and variation of O₃ were deemed reasonably reproduced (He et al., 2019; Liu et al., 2021; Wang et al., 2018b; Wang et al., 2017; Wang et al., 2015).

$$180 \quad IOA = 1 - \frac{\sum_{i=1}^n (O_i - S_i)^2}{\sum_{i=1}^n (|O_i - \bar{O}| + |S_i - \bar{O}|)^2} \quad (1)$$

Where O_i and S_i represent the measured and simulated O₃ concentration, respectively; \bar{O} represents the mean measured O₃ concentration; and n represents the number of samples. The index of IOA typically ranges from 0 to 1, with higher values indicating stronger alignment between simulation and observation.

185 Dominant photochemical production pathways (HO₂ + NO, RO₂ + NO) and destruction pathways (O₃ photolysis, O₃ + OH, O₃ + HO₂, VOCs + O₃, NO₂ + OH) of O₃ were determined using Equations 2-4 (Tan et al., 2019a; Wang et al., 2018a). The production rates of RO_x radicals (OH, HO₂ and RO₂ radicals) were also calculated, incorporating primary sources such as photolysis reactions (i.e., O₃ photolysis, OVOC photolysis, etc.), VOC reactions with O₃
190 and NO₃, as well as recycling processes (Xue et al., 2016; Wang et al., 2018a; Tan et al., 2019b).

To evaluate the model uncertainties associated with the presence of multiple isomers in PTR-ToF-MS measurements, we conducted a sensitivity analysis by estimating the lower and upper limits of RO_x radicals and O₃ production rates with possible isomers. In this analysis, each OVOC molecular formula was assigned either to the isomer with the minimum or
195 maximum photolysis frequencies and K_{OH} values among all plausible isomeric structures. This approach accounts for the variability in chemical reactivity stemming from the unresolved



isomer distribution and provides a range of potential impacts on atmospheric RO_x radicals generation and O₃ formation.

$$P(O_3) = k_{HO_2+NO}[HO_2][NO] + \sum k_{RO_2+NO}[RO_2][NO] \quad (2)$$

$$L(O_3) = k_{O(^1D)+H_2O}[O(^1D)][H_2O] + k_{O_3+OH}[O_3][OH] + k_{O_3+HO_2}[O_3][HO_2] + \sum k_{O_3+VOCs}[O_3][VOCs] + k_{NO_2+OH}[NO_2][OH] \quad (3)$$

$$Net P(O_3) = P(O_3) - L(O_3) \quad (4)$$

Where $P(O_3)$, $L(O_3)$, and $Net P(O_3)$ represents the production rate, loss rate, and net production rate of O₃, respectively. The O₃ photolysis was represented as the reactions of O(¹D) and H₂O (Shen et al., 2021). VOCs here included both constrained VOCs and model simulated VOCs. The constants (k) represent the rate coefficients of each reaction.

The O₃-precursors relationship was characterized using the relative incremental reactivity (RIR) method, calculated by Equation 5 (Liu et al., 2021). O₃ formation regime was further characterized by O₃ isopleth method, which was derived by scaling precursor concentrations (10%-200% of original values) to simulate O₃ concentrations under varying VOCs and NO_x levels (Tan et al., 2018).

$$RIR(X) = \frac{[P_{O_3-NO}(X) - P_{O_3-NO}(X-\Delta X)] / P_{O_3-NO}(X)}{\frac{\Delta S(X)}{S(X)}} \quad (5)$$

Where RIR represents relative incremental reactivity; X represents specific O₃ precursor (i.e., VOCs, NO_x); S(X) represents observed concentration of precursor X (ppbv); $\Delta S(X)$ represents hypothetical change of the concentration of precursor X; $P_{O_3-NO}(X)$ represents net O₃ production in a base run with original observed precursor concentrations, while $P_{O_3-NO}(X-\Delta X)$ represents the net O₃ production in a second run with a hypothetical change $\Delta S(X)$ of 10% in this study. The net O₃ production was calculated by Equation 4. A larger positive RIR value indicates higher sensitivity of O₃ production to this precursor, implying that reducing emissions of this precursor would more effectively suppress O₃ formation. Conversely, a negative RIR value suggests that emission reductions of this precursor could paradoxically increase O₃ production (Wang et al., 2018b).

3. Results and discussion

3.1 Overview of the observations

During the campaign, 117 VOC/OVOC species were continuously measured using the PTR-ToF-MS, including 2 biogenic VOCs (BVOCs), 24 anthropogenic VOCs (AVOCs),



comprising alkenes, cycloalkanes, and aromatics), 63 OVOCs (categorized as $C_xH_yO_{1-3}$), and 28 nitrogen/sulfur containing VOCs (N/S-containing VOCs). The time series of different VOC groups, meteorological parameters, and trace gases are shown in Figure S1. The campaign
230 witnessed twenty O_3 episode days (maximum O_3 value > 80 ppbv) across three seasons, with three extreme episodes exceeding 110 ppbv (defined as high- O_3 episodes) in summer. The measured VOCs/OVOCs showed the highest total concentration in early winter (47.84 ppbv), followed by autumn (44.26 ppbv) and summer (28.83 ppbv), which is consistent with the O_3 seasonal trend (Figure S4). Furthermore, the total VOCs/OVOCs concentration was much
235 higher during O_3 episode days and reached 60.96 ppbv during summer high- O_3 episode days, with 76% contribution from OVOCs, emphasizing their pivotal role in O_3 production. OVOCs, AVOCs, and N/S-containing VOCs increased progressively from summer to early winter, with the most pronounced rise observed between summer and autumn (Figure 1a). In contrast, BVOCs displayed an opposite seasonal pattern, with concentrations peaking in summer.
240 OVOCs were the dominant group across all seasons, accounting for 72%-77% of the total concentration, with $C_xH_yO_1$ and $C_xH_yO_2$ accounting for 51%-53% and 17%-24%, respectively (Figure 1b). CH_4O was the most abundant OVOC species, with average concentration ranging from 5.98-10.10 ppbv across seasons, followed by $C_2H_4O_2$ (1.91-5.75 ppbv), C_3H_6O (4.22-5.67 ppbv) and C_2H_4O (1.85-3.86 ppbv), as shown in Figure S2. A statistical summary of
245 VOC/OVOC concentrations for each season is provided in Table S2.

The diurnal variations of OVOC subgroups across three seasons are shown in Figure 1c. $C_xH_yO_{1-3}$ groups displayed similar diurnal patterns in different seasons, characterized by pronounced daytime enhancements, particularly for species such as C_2H_4O , C_3H_6O , C_4H_6O and $C_2H_4O_2$ (Figure S3). These species increased at about 7:00 local time (LT), peaked during
250 12:00-17:00 LT in the afternoon, and then gradually decreased, which was aligned closely with the diurnal patterns of O_3 (Figure S4), indicating their likely formation through photochemical reactions. Notably, C_4H_6O (methyl vinyl ketone and methacrolein), the key oxidation products of isoprene (Li et al., 2021), showed pronounced photochemical daytime peaks but significantly higher concentrations in summer compared to autumn and early winter, consistent
255 with the seasonal trend of its precursor (Figure S5), which was different from other OVOCs formed by anthropogenic precursors. CH_4O exhibited clear daytime enhancements in summer and autumn but showed no distinct diurnal pattern in early winter (Figure S3). Instead, it maintained relatively high levels throughout the day and night in early winter, likely reflecting the larger contributions from regional background sources, such as anthropogenic emissions
260 and background transport (Brito et al., 2015; Huang et al., 2019). These findings underscore



the significance of OVOCs in atmospheric chemistry, given their abundance and complex roles in photochemical reactions.

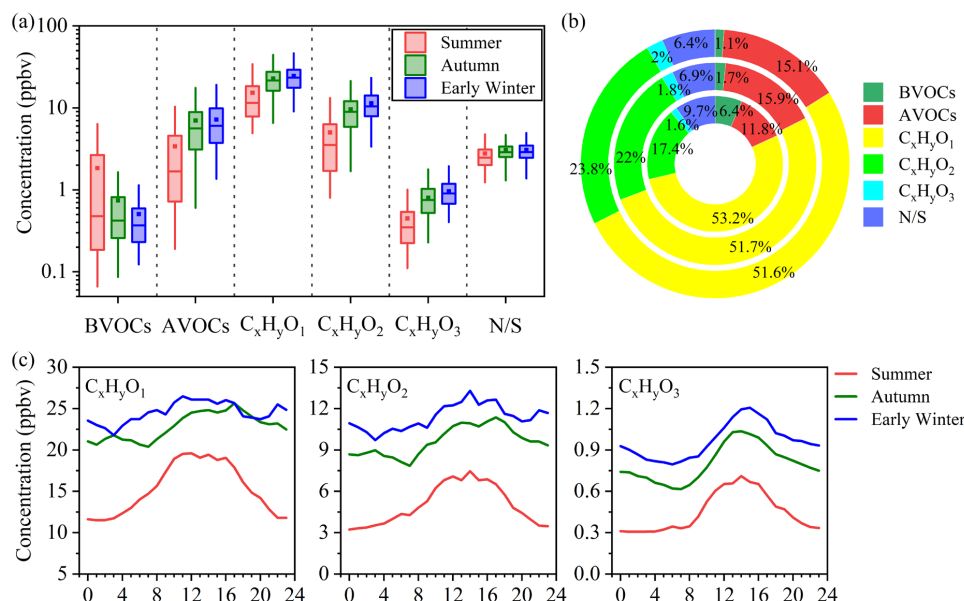


Figure 1. (a) The concentrations of different VOC groups in summer, autumn and early winter. The box plots show mean values (square), median (line within the box), interquartile range (IQR, 25%-75%), and whiskers extending to $\pm 1.5 \times \text{IQR}$. (b) The contributions of different VOC groups to total concentration in summer (inner), autumn (middle), and early winter (outer). (c) Diurnal variations of OVOC subgroups across three seasons.

3.2 O₃-precursor relationships

To further evaluate the contribution of various VOCs to O₃ formation, the RIR values of key O₃ precursors (including BVOCs, AVOCs, OVOCs, and NO_x) were calculated for different seasons based on the model simulations. It should be noted that the subgroups of OVOCs and AVOCs analyzed here differ slightly from those in Section 3.1, due to the limitations that MCM does not include all mechanisms for all observed OVOC species. Additionally, C₂-C₁₀ hydrocarbons measure by GC-MS/FID/ECD were also included in the subgroup of AVOCs for this analysis. The species included in RIR calculation comprised 3 BVOC species, 45 AVOC species and 63 OVOC species, with detailed information summarized in Table S4.

The RIR values for all VOCs subgroups and NO_x were positive across three seasons (Figure 2a), indicating a transition regime of O₃ formation in the study region and that reduction



in VOCs and/or NO_x would lead to decreases in O₃ levels. This result was different from previous studies which reported dominantly VOC-limited regime of O₃ formation in Hong Kong (Liu et al., 2021; Zhang et al., 2007; Cheng et al., 2010; Guo et al., 2013). In summer, NO_x exhibited the highest RIR value (0.65), followed by BVOCs (0.21) and OVOCs (0.16). Similar trend was observed during high-O₃ episode days (Figure S6), indicating that summer O₃ formation is more sensitive to NO_x. By contrast, in autumn and early winter, OVOCs exhibited the highest RIR values (0.42-0.48), followed by NO_x (0.25-0.35) and BVOCs (0.14-0.16), indicating that O₃ formation in these seasons is more sensitive to OVOCs. The dramatic seasonal increase in the RIR value of OVOCs, coupled with a decline in those of NO_x highlights the need for different control strategies to effectively reduce O₃ levels depending on the seasons. Previous RIR studies of O₃ formation have primarily focused on AVOCs, BVOCs and NO_x, with limited consideration of OVOCs (Wang et al., 2018b; Tan et al., 2018; Wang et al., 2022b; Yu et al., 2020; Zhang et al., 2008; Lin et al., 2020; Zhao et al., 2020; Guo et al., 2022). Recent studies, however, have reported relatively high RIR values for OVOCs when they are included in the simulations, although these findings are confined to a narrow subset of OVOCs, mainly short-chain carbonyl compounds, based on low-resolution offline measurements (Shen et al., 2021; Yang et al., 2018; Wang et al., 2024; Feng et al., 2023). This study integrates a much broader spectrum of OVOCs (including aldehydes, ketones, organic acids, alcohols, phenolic compounds, etc.) supported by high-resolution measurement into the observation-constrained modeling framework. This improved chemical comprehensiveness allows for a more robust characterization of OVOCs reactivity, particularly their contributions to radical production and O₃ sensitivity.

In addition, we have further examined the diurnal variation of RIR values for O₃ precursors in different seasons, as shown in Figure 2b. Significantly higher positive RIR values was observed for NO_x than other precursors in the afternoon of summer and during the episodes (Figure S7), indicating a consistently strong sensitivity of O₃ production to NO_x. In autumn and early winter, OVOCs exhibited higher positive RIR values during the morning (9:00-11:00) and midday (11:00-14:00), underscoring their prominent role in O₃ formation. The majority of NO_x RIR values were positive except for the negative values in the morning (9:00-11:00), reflecting a shift from a VOC-limited regime in the morning to a transitional regime at the noon and in the afternoon. By late afternoon, the O₃ formation regime became increasingly sensitive to NO_x. Notably, in autumn, RIR values of NO_x were comparable or even surpassed these of OVOCs in the afternoon. This variation is likely attributed to fresh NO_x emissions from vehicle and/or household combustion activities in the morning, which decrease in the afternoon due to



photochemical consumption, atmospheric diffusion, and dry deposition in the afternoon (Liu et al., 2021). These findings indicate a clear diurnal transformation pattern in O₃ formation regimes during the photochemical active seasons (autumn and early winter) in Hong Kong. Specifically, the regime transitions from VOC-limited in the morning to a transitional regime with higher sensitivity to OVOCs at midday, and then to a general transitional regime with sensitivity to both OVOCs and NO_x in the afternoon, and becomes increasingly NO_x sensitive by late afternoon.

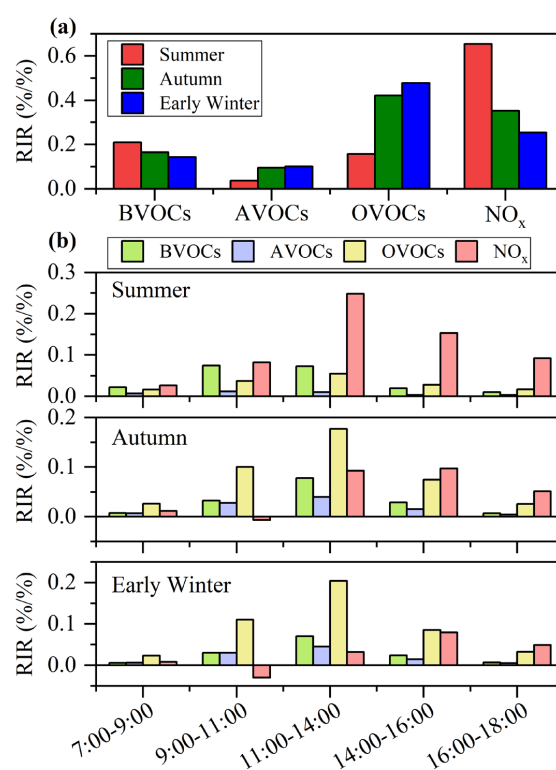


Figure 2. (a) Average RIR values of O₃ precursors (BVOCs, AVOCs, OVOCs, and NO_x) during summer, autumn and early winter. (b) Diurnal patterns of RIR values for O₃ precursors across summer, autumn and early winter.

3.3 O₃ formation mechanism and radical budget

The main pathways of daytime O₃ production and destruction in three seasons were further explored using the photochemical box model, as shown in Figure S8. The daytime average net O₃ production rate (P_{net}) was 5.8 ppbv/h, 6.1 ppbv/h, and 6.4 ppbv/h in summer, autumn, and early winter, respectively, much lower than that during summer high-O₃ episode (13.1 ppbv/h, Figure S8b). These trends were consistent with the diurnal patterns of observed



O₃ concentrations (Figure S9). Daytime O₃ production (P(O₃)) was dominated driven by the
335 reactions of HO₂ + NO and RO₂ + NO, contributing 43.8%-53.0% and 47.0%-56.2%,
respectively. Among the diverse RO₂ + NO reactions (involving over 1000 different RO₂
radicals), the top 10 pathways contributed 51.1%-54.3% of the total production rates (Figure
S10). CH₃O₂ + NO was the dominant pathway, accounting for 13.5%-19.3% of O₃ production.
The CH₃O₂ radical could be generated through various reactions, including the photolysis of
340 OVOCs (e.g., acetaldehyde, acetone) and VOCs reactions with OH radical (e.g., acetic acid),
etc. Additionally, reactions of C₂ radicals with NO contributed significantly (10.4%-18.5%),
with CH₃CO₃ + NO being the most prominent (10.4%-15.2%). Seasonal variations in RO₂ +
NO pathways were evident. RO₂ radicals from BVOCs (such as isoprene and pinenes)
contributed more to summer (20.7%) than autumn and early winter (6.3%-6.9%), reflecting the
345 seasonal patterns of vegetation emissions. Conversely, RO₂ radicals derived from
anthropogenic sources, such as aromatics, played a larger role in autumn and early winter
(8.6%-9.1%). Daytime O₃ destruction also exhibited seasonal differences. In autumn and early
winter, the dominant loss pathway was OH + NO₂ (51.1%-57.0%), followed by VOCs + O₃
(17.9%-23.2%) and O₃ + HO₂ (12.6%-13.8%). In summer, however, VOCs + O₃ accounted for
350 a much higher fraction of O₃ loss (43.3%) compared to other seasons, especially the reactions
with BVOCs including α -pinene and isoprene.

The OH, HO₂, and RO₂ radicals play important roles in the initiation and propagation
of atmospheric photochemical reactions (Wang et al., 2022b). The daytime production budgets
of these radicals were analyzed across three seasons, as shown in Figure S11, with detailed
355 contributions of each pathway presented in Figure 3. Daytime OH and HO₂ radical production
was highest in early winter, with lower values in summer and autumn. Radical recycling via
HO₂ + NO was the dominant source of OH production (86.4%-94.4%) across three seasons,
while O₃ photolysis (via O(¹D) + H₂O) served as the main primary source for OH production,
accounting for around 60% of primary OH production rate. In addition, the photolysis reactions
360 of OVOCs, HONO and VOCs + O₃ contributed 7.6%-18.3%, 2.7%-20.4%, and 9.3%-15.6%
of primary OH production rates, respectively. Similarly, the largest source of HO₂ radicals was
radical recycling through RO₂ + NO reactions, contributing 42.5%-50.2%. OVOC photolysis
accounted for 20.3%-21.0% to total HO₂ production rates, but dominated the primary HO₂
production in three seasons (95.2%-98.6%). Moreover, the reactions of OVOCs + OH (15.4%-
365 17.7%) and CO + OH (10.2%-18.7%) also played significantly roles in total HO₂ production.
The dominant source of daytime RO₂ production was the reaction of VOCs + OH, accounting
for 50.8%-61.1%, with OVOCs + OH contributing the majority proportion (41.2%-51.3%).



Seasonal variations in OVOCs + OH contributions aligned with observed OVOC concentrations, being highest in early winter, followed by autumn and summer. Additional RO₂ sources included RO decomposition (13.9%-21.3%), OVOC photolysis (10.0%-14.2%), and VOCs + NO₃ (9.6%-14.1%). OVOC photolysis was also an important primary source of daytime RO₂ production (36.0%-57.0%). During summer high-O₃ episodes, daytime RO_x radical production rates were significantly higher, and O₃ photolysis and VOCs + O₃ reactions contributed more substantially to RO_x production (Figure S12). Furthermore, the results highlight the importance of VOCs + NO₃, especially OVOCs + NO₃, as a source of RO₂ radicals in the daytime photochemistry, particularly in polluted atmosphere, consistent with prior observations at an urban site in Hong Kong (Xue et al., 2016). In total, OVOCs played a significant role in the formation of HO₂ and RO₂ radicals across all three seasons. OVOC-related reactions, including OVOC photolysis, OVOCs + OH oxidation, and OVOCs + NO₃, accounted for 36.4%-38.5% and 59.1%-73.4% of daytime HO₂ and RO₂ production, respectively. These results emphasize the critical importance of OVOCs in sustaining radical cycling and driving photochemical O₃ formation, especially in urban and semi-urban atmospheric environments.

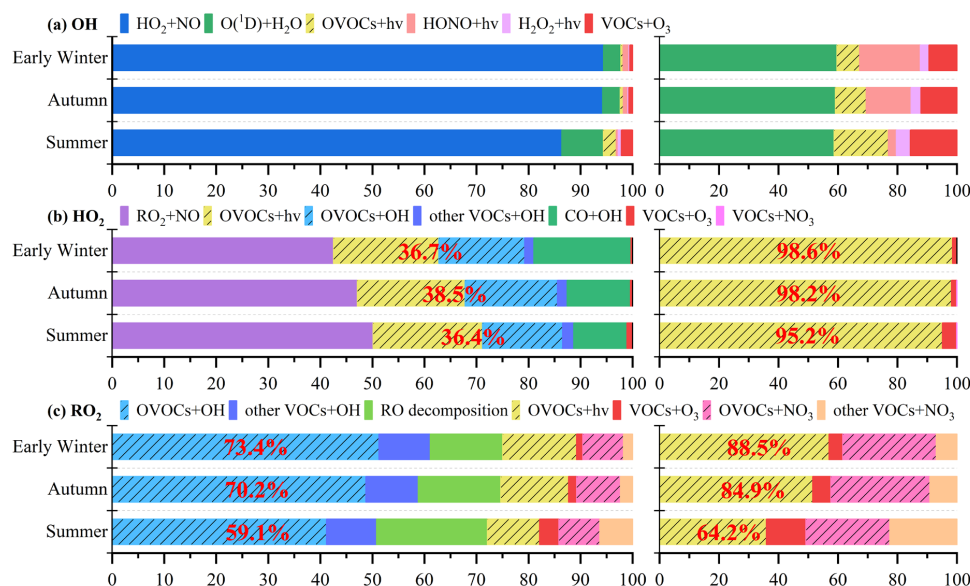


Figure 3. Contributions of key pathways for total daytime production rates (left) and primary daytime production rates (right) of (a) OH, (b) HO₂ and (c) RO₂ radicals across seasons. OVOC-related reactions including OVOC photolysis (OVOCs + hν), OVOCs oxidation by OH radicals (OVOCs + OH), and OVOCs oxidation by NO₃ (OVOCs + NO₃) are shaded by oblique lines. The percentage in red represents the contribution of OVOC-related reactions for overall (left) and primary (right) daytime production rates of HO₂ and RO₂ radicals.



3.4 Importance of OVOCs in O₃ and radical formation

To better quantify the critical roles of OVOCs in photochemical O₃ and radical formation, a sensitivity simulation was conducted without constraining the observed OVOC species in the model. The comparison of observed and simulated O₃ concentrations under scenarios with and without OVOCs constraints across three seasons is shown in Figure S13. The simulation with OVOCs constraints successfully reproduced the observed O₃ concentrations in all seasons. However, without OVOCs constraints, daytime O₃ concentration were underestimated by 26.5% in autumn and 35.7% in early winter. The discrepancy was smaller in summer, with only minimal differences between two scenarios. This reduced sensitivity in summer is likely associated with the dominant role of NO_x in O₃ formation in this season, coupled with elevated daytime NO concentrations, particularly during high-O₃ episodes. Given that O₃ levels were higher in early winter than other seasons and that substantial underestimations of O₃ were found without considering OVOCs, a detailed analysis of model performance was conducted for this period.

As shown in Figures 4a and 4b, simulated daytime P(O₃) and P_{net} without OVOCs constraints decreased by 44.0% and 45.1%, significantly, compared to the constrained scenario in early winter, consistent with the underestimation of O₃ concentration in the same period. The underestimation in RO₂ + NO reaction rates (45.6%) was slightly larger than that for HO₂ + NO (42.6%), with substantial underestimation observed for the top two RO₂ pathways: CH₃O₂ + NO (61.4%) and CH₃CO₃ + NO (58.6%) (Figure 4c). These discrepancies were primarily attributed to the underestimation of precursors required for RO₂ and HO₂ radical production without OVOCs constraints. Moreover, the existence of various OVOCs isomers, as detected by PTR-ToF-MS, introduces additional uncertainties in quantifying daytime O₃ production. Sensitivity analysis revealed that P_{net} underestimations without OVOCs constraints ranged from 43.4% to 52.1%, depending on whether the minimum and maximum photolysis frequencies or K_{OH} values of potential isomers were assumed (Figure 4d). The substantial underestimations of O₃ without OVOCs constraints underscore the critical role of OVOCs in O₃ formation and highlight the potentially large uncertainties in O₃ modeling when their contributions are inadequately represented. The differences are significantly larger than those reported in previous studies (Wang et al., 2022a; Shen et al., 2021), and likely arise from our inclusion of a wider range of OVOCs beyond the typically considered carbonyls. This enhances



the chemical completeness of the model, thereby reducing uncertainties and improving the accuracy of O₃ formation simulations.

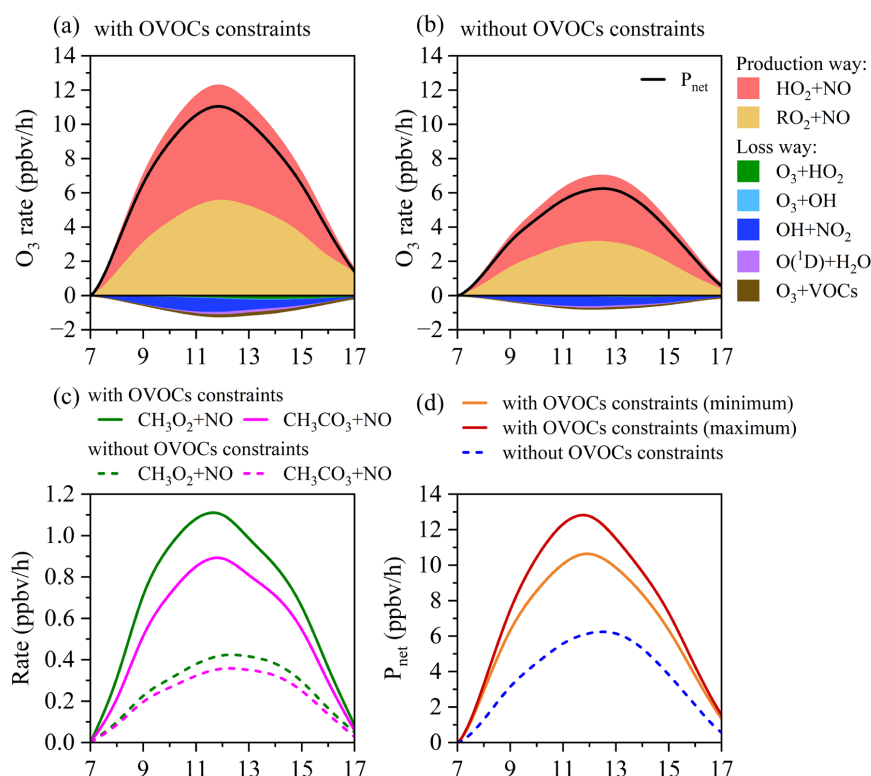


Figure 4. Model simulated daytime O₃ production and loss rates of main pathways in early winter (a) with and (b) without observed OVOCs constraints. The black solid line represents the net O₃ production rate (P_{net}). (c) The daytime reaction of the top two pathways of RO₂ + NO (CH₃O₂ + NO, CH₃CO₃ + NO) towards daytime O₃ formation in early winter with and without OVOCs constraints. (d) The daytime P_{net} with and without observed OVOCs constraints in early winter. The orange and dark red lines represent the scenarios with the minimum and maximum OVOC contributions to P_{net}, respectively.

The critical role of OVOCs in modulating atmospheric radical budgets was further quantified through scenario-based simulations. As illustrated in Figure 5a, without OVOCs constraints, the production rates of OH, HO₂ and RO₂ radicals decreased significantly, with underestimations of 41.4% (40.2%-47.4% considering the minimum and maximum scenarios), 44.4% (43.2%-51.0%), and 48.0% (45.8%-57.1%), respectively. These underestimations were amplified in OVOC-related reactions, where HO₂ and RO₂ production were reduced by 58.3% (58.1%-65.5%) and 64.1% (62.0%-72.2%), respectively, underscoring the significance of OVOCs in radical cycling. These reductions were primarily attributed to the underestimation



of OVOC photolysis (37.4%-64.5%) and OVOCs + OH reactions (60.0%-71.0%) (Figure 5b). Although some carbonyl compounds are typically included in models of radical formation (Zhao et al., 2020; Yu et al., 2020; Chen et al., 2023; Han et al., 2023; Huang et al., 2020a; Liu et al., 2019; Liu et al., 2022), our results highlight that many other OVOCs, particularly those
445 reactive to OH oxidation and photolysis, remain overlooked, contributing to large uncertainty in simulated radical budgets. Furthermore, prominently large underestimations (up to 93.6%-95.0%) were observed for OVOCs + NO₃ reactions to RO₂ production (Figure 5b), which signals a critical gap in modeling daytime NO₃ oxidation chemistry of OVOCs. The significantly large underestimations of the production rates of RO_x radicals and OVOC-related
450 reactions were mainly due to the underestimation of OVOC concentrations simulated by the photochemical model. Key OVOC species such as methanol, acetaldehyde and acetone, which are dominant and photodegradable species, were underestimated by 73%-99% in the simulations without OVOC constraints in early winter (Table S5). Similar underestimation of 10-100% of simulated OVOCs have been reported in previous studies (Wang et al., 2022a).
455 The missing or underestimated OVOC in these simulations may be linked to unidentified primary emission sources or unaccounted secondary sources, as current chemical mechanism, including the MCM, do not fully represent all OVOC pathways (Karl et al., 2018; Mo et al., 2016; Bloss et al., 2005). This highlights the essential role of broader OVOCs constraints in accurately representing atmospheric radical budgets and O₃ formation. However, even with
460 expanded inclusion of OVOCs in this study, certain OVOC species could not be precisely quantified, introducing residual uncertainties. Therefore, further advancements in measurement techniques are imperative to achieve more accurate OVOC quantification and reduce modeling uncertainties.

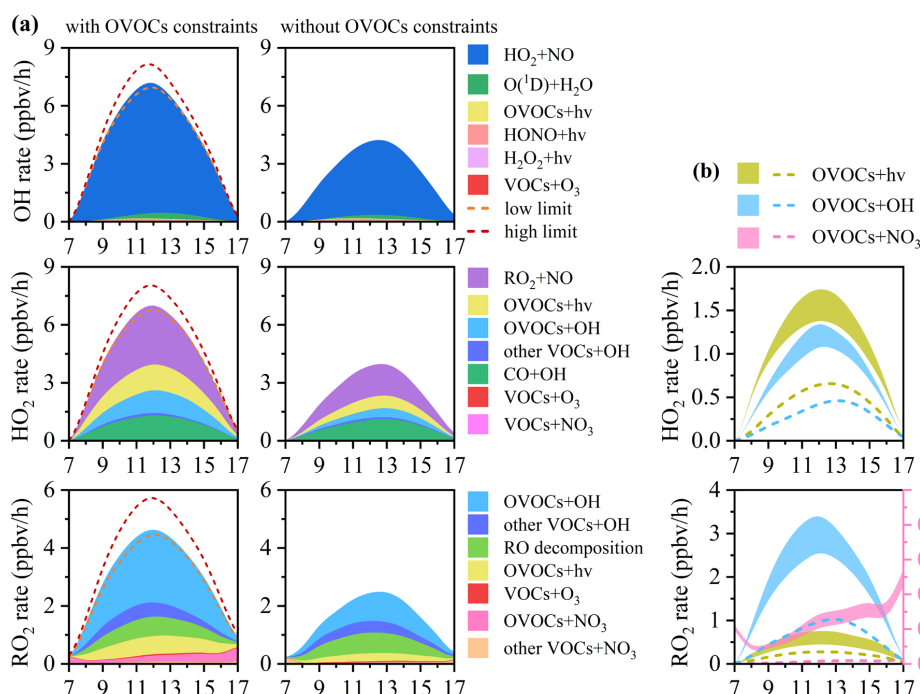


Figure 5. (a) Model simulated daytime production rates of OH, HO₂ and RO₂ radicals of main pathways in early winter with (left) and without (right) observed OVOCs constraints. The orange and dark red dash lines represent daytime production rates with minimum and maximum scenarios, respectively. (b) The reaction rates of OVOC photolysis (OVOCs + hv), OH oxidation of OVOCs (OVOCs + OH), and NO₃ oxidation of OVOCs (OVOCs + NO₃) towards daytime production of HO₂ and RO₂ radicals in early winter. The dash lines represent the scenario without OVOCs constraints. The areas represent daytime production rates with minimum and maximum scenarios.

3.5. Implication for O₃ pollution control strategies

Given the significant roles of OVOCs in O₃ production, EKMA O₃ isopleths were derived to evaluate the dependence of daytime O₃ production on VOCs and NO_x variations. The isopleth analysis revealed a critical difference between the two scenarios: suburban Hong Kong was classified in the transition regime with OVOCs included as constraints (Figure 6a), whereas the region shifted to a VOC-limited regime without OVOCs constraints (Figure 6b). This shift highlights the importance of including OVOCs in modeling efforts, as the exclusion of OVOCs could lead to different and potentially misleading strategies for O₃ pollution control. Figure 6c further illustrates changes in daytime O₃ production in response to VOCs or NO_x reductions (0% to 90%) under the two scenarios. When OVOCs were considered, O₃



concentration would decrease with the reduction of VOCs or NO_x but more rapidly with VOCs,
485 consistent with the transition regime. In contrast, without OVOCs constraints, O₃ concentration
would initially increase with NO_x reduction of 0%-50%, before declining at higher reductions.
Similar trends were observed in changes to daytime production rates of O₃ and RO_x radicals,
as shown in Figure S14. Therefore, model simulation without OVOCs constraints will
overestimate the VOC-limited degree and thus overestimate the impact of VOCs reduction on
490 O₃ reduction, which may lead to incorrect policy implications on O₃ pollution control,
particularly on NO_x reduction. This response suggests that the absence of OVOCs constraints
exaggerates the degree of VOC limitation, overestimating the impact of VOC reductions on O₃
control while underestimating the potential effects of NO_x reduction.

For regions in the transition regime, such as suburban Hong Kong, simultaneous
495 reductions of both VOCs and NO_x are necessary for effective O₃ control. The optimal reduction
ratios of VOCs and NO_x, along with the response of daytime O₃ concentration, were simulated
and shown in Figure 6d. When VOCs reduction is between 0% and 40%, any reduction in NO_x
would result in a corresponding reduction in O₃ concentration. However, when VOCs reduction
reaches 60%-90%, minor NO_x reductions would paradoxically increase the O₃ concentration
500 unless NO_x reduction is sufficiently large to outweigh the VOCs reductions. When NO_x
reduction exceeds 90%, O₃ concentration would be reduced to below 25 ppbv, regardless of
VOC reductions. While achieving such substantial reductions in either VOCs or NO_x emissions
presents practical challenges, a dual-focus strategy emerges as the most viable approach.
Specifically, reducing VOC emissions by 0%-40% while simultaneously minimizing NO_x
505 emissions as much as possible is both pragmatic and effective. This dual strategy balances
feasibility with impact, ensuring significant O₃ reductions without introducing
counterproductive effects from disproportionate reductions in either precursor.

Although this study was conducted in a representative suburban region in Hong Kong,
the methodology and findings are broadly transferable to other urban and suburban regions
510 with diverse emission profiles and photochemical regimes, particularly in areas influenced by
both biogenic and anthropogenic sources. Excluding OVOCs in such environments can lead to
misclassification of O₃ formation regimes, resulting suboptimal or even counterproductive
mitigation efforts, especially where OVOCs remain undermeasured and underrepresented in
models. These insights underscore the critical need for OVOCs-inclusive modeling
515 frameworks to guide effective and science-based air quality management.

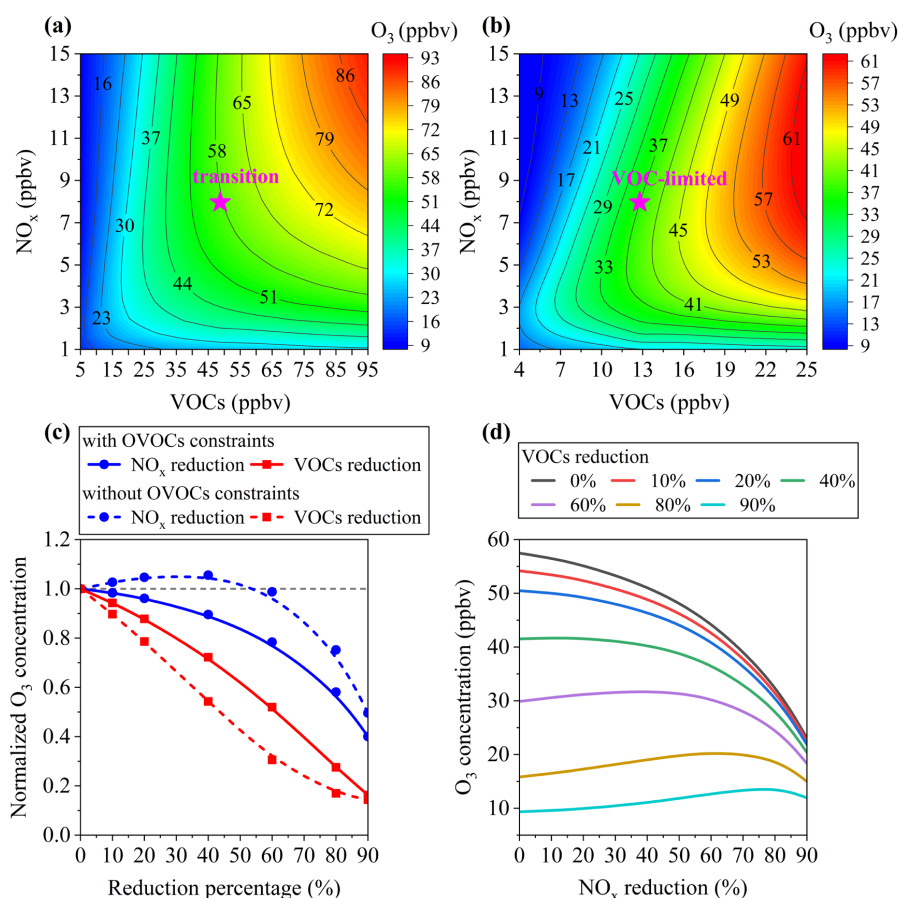


Figure 6. Isopleth diagram for average daytime O_3 production depending on NO_x and VOCs changes in early winter (a) with and (b) without observed OVOCs constraints. The “pink star” represents the base scenario. (c) Changes in daytime O_3 production with VOCs or NO_x reductions from 0% to 90% with and without observed OVOCs constraints. The daytime average O_3 concentrations were normalized to the corresponding values in the base run. The grey dash line represents the normalized O_3 concentration of 1.0, indicating no O_3 changing. (d) The response of daytime O_3 concentration to VOCs and NO_x under different reduction scenarios with observed OVOCs constraints.

4. Conclusions

This study integrated intensive field measurements with observation-based photochemical modeling to investigate the role of OVOCs in O_3 and radical chemistry at a coastal suburban site in subtropical Hong Kong. High-resolution measurements using PTR-ToF-MS identified and quantified 117 VOC/OVOC species, among which 63 OVOCs contributed the majority (72%–77%) of total VOC concentrations across three seasons in 2021.



RIR analysis revealed a transitional O₃ formation regime in this suburban region, with heightened sensitivity to OVOCs, especially in autumn and early winter. Notably, O₃-precursor relationship also showed diurnal variations, transitioning from a VOC-limited regime in the morning to a transitional regime during midday and afternoon, underscoring the dynamic nature of O₃ chemistry.

Photochemical modeling demonstrated that OVOC-related reactions, including photolysis and oxidation by OH and NO₃ radicals, contributed substantially to radical formation, accounting for 36.4%-38.5% of daytime HO₂ and 59.1%-73.4% of RO₂ radical production. Importantly, simulations without comprehensive OVOC constraints would significantly underestimate daytime O₃ and RO_x production rates by 41%-48% and incorrectly diagnosed the O₃ chemical regime. Such misclassification may lead to misguided control strategies. Compared with previous studies that only focused on a limited set of carbonyls using offline techniques, this study expands the chemical scope by including a broader suite of OVOCs through high-resolution, real-time measurements, providing a more complete assessment of OVOC-driven radical and O₃ formation. The mechanistic insights and modeling framework developed here offer practical value for diagnosing O₃ formation sensitivity and designing more effective air quality management strategies in chemically complex environments globally.

Overall, these findings underscore the critical role of OVOCs in shaping atmospheric oxidation capacity and O₃ formation, and highlight the need for integrating high-resolution, chemically comprehensive OVOC measurements into photochemical models. Doing so will improve the accuracy of O₃ formation regimes classification, reduces uncertainties in radical budgets, and supports the development of targeted, science-based, and sustainable O₃ pollution control strategies at both regional and global scales.

Data availability

The datasets associated with the current study are available from the corresponding author [z.wang@ust.hk] on reasonable request.

Author contributions

L.H. conducted field measurement, data analysis, model simulations and wrote the paper. Y.C. assisted in supervising the paper and provided feedback on the analysis and manuscript. D.G.



565 and H.S. provided VOC data measured by GC-MS/FID/ECD for model simulation. J.G. and
Y.C. provided help with model simulations. X.F., Y.X., and P.Z. provided feedback on the
analysis and manuscript. Z.W. supervised the paper and supported the funding. All the authors
participated in reviewing and editing the final version of the paper.

570 **Competing interests**

The authors declare that they have no conflict of interest.

Supporting information

The Supporting Information is available free of charge.

575 **Acknowledgement**

The authors would like to acknowledge the Environmental Central Facility of HKUST for
providing the air quality supersite and equipment support on ambient measurement.

Financial support

580 This study is supported by National Natural Science Foundation of China (42122062), the
Research Grants Council (RGC) of Hong Kong Special Administrative Region, China
(16209022, 16201623, 16211824), Hong Kong Environment and Conservation Fund (project
102/2023), and Guangdong Natural Science Foundation (GDST23SC13).

585 **References**

- Bloss, C., Wagner, V., Bonzanini, A., Jenkin, M. E., Wirtz, K., Martin-Reviejo, M., and Pilling,
M. J.: Evaluation of detailed aromatic mechanisms (MCMv3 and MCMv3.1) against
environmental chamber data, *Atmos. Chem. Phys.*, 5, 623–639, 2005.
- 590 Brito, J., Wurm, F., Yanez-Serrano, A. M., de Assuncao, J. V., Godoy, J. M., and Artaxo, P.:
Vehicular Emission Ratios of VOCs in a Megacity Impacted by Extensive Ethanol Use: Results
of Ambient Measurements in Sao Paulo, Brazil, *Environ Sci Technol*, 49, 11381–11387,
10.1021/acs.est.5b03281, 2015.
- Chai, W., Wang, M., Li, J., Tang, G., Zhang, G., and Chen, W.: Pollution characteristics,
sources, and photochemical roles of ambient carbonyl compounds in summer of Beijing, China,
595 *Environ Pollut*, 336, 122403, 10.1016/j.envpol.2023.122403, 2023.
- Chen, J., Liu, T., Gong, D., Li, J., Chen, X., Li, Q., Liao, T., Zhou, Y., Zhang, T., Wang, Y.,
Wang, H., and Wang, B.: Insight into decreased ozone formation across the Chinese National
Day Holidays at a regional background site in the Pearl River Delta, *Atmos. Environ.*, 315,
10.1016/j.atmosenv.2023.120142, 2023.



- 600 Chen, T., Xue, L., Zheng, P., Zhang, Y., Liu, Y., Sun, J., Han, G., Li, H., Zhang, X., Li, Y., Li, H., Dong, C., Xu, F., Zhang, Q., and Wang, W.: Volatile organic compounds and ozone air pollution in an oil production region in northern China, *Atmos. Chem. Phys.*, 20, 7069-7086, 10.5194/acp-20-7069-2020, 2020.
- Cheng, H., Guo, H., Wang, X., Saunders, S. M., Lam, S. H., Jiang, F., Wang, T., Ding, A., Lee, S., and Ho, K. F.: On the relationship between ozone and its precursors in the Pearl River Delta: application of an observation-based model (OBM), *Environ. Sci. Pollut. Res. Int.*, 17, 547-560, 10.1007/s11356-009-0247-9, 2010.
- Ding, A., Wang, T., and Fu, C.: Transport characteristics and origins of carbon monoxide and ozone in Hong Kong, South China, *Journal of Geophysical Research: Atmospheres*, 118, 9475-9488, 10.1002/jgrd.50714, 2013.
- 610 Feng, X., Guo, J., Wang, Z., Gu, D., Ho, K.-F., Chen, Y., Liao, K., Cheung, V. T. F., Louie, P. K. K., Leung, K. K. M., Yu, J. Z., Fung, J. C. H., and Lau, A. K. H.: Investigation of the multi-year trend of surface ozone and ozone-precursor relationship in Hong Kong, *Atmos. Environ.*, 315, 10.1016/j.atmosenv.2023.120139, 2023.
- 615 Feng, Z., De Marco, A., Anav, A., Gualtieri, M., Sicard, P., Tian, H., Fornasier, F., Tao, F., Guo, A., and Paoletti, E.: Economic losses due to ozone impacts on human health, forest productivity and crop yield across China, *Environ. Int.*, 131, 104966, 10.1016/j.envint.2019.104966, 2019.
- Guo, H., Ling, Z. H., Cheung, K., Jiang, F., Wang, D. W., Simpson, I. J., Barletta, B., Meinardi, S., Wang, T. J., Wang, X. M., Saunders, S. M., and Blake, D. R.: Characterization of photochemical pollution at different elevations in mountainous areas in Hong Kong, *Atmos. Chem. Phys.*, 13, 3881-3898, 10.5194/acp-13-3881-2013, 2013.
- Guo, W., Yang, Y., Chen, Q., Zhu, Y., Zhang, Y., Liu, Y., Li, G., Sun, W., and She, J.: Chemical reactivity of volatile organic compounds and their effects on ozone formation in a petrochemical industrial area of Lanzhou, Western China, *Sci Total Environ*, 839, 155901, 10.1016/j.scitotenv.2022.155901, 2022.
- 625 Han, C., Liu, R., Luo, H., Li, G., Ma, S., Chen, J., and An, T.: Pollution profiles of volatile organic compounds from different urban functional areas in Guangzhou China based on GC/MS and PTR-TOF-MS: Atmospheric environmental implications, *Atmos. Environ.*, 214, 10.1016/j.atmosenv.2019.116843, 2019.
- 630 Han, J., Liu, Z., Hu, B., Zhu, W., Tang, G., Liu, Q., Ji, D., and Wang, Y.: Observations and explicit modeling of summer and autumn ozone formation in urban Beijing: Identification of key precursor species and sources, *Atmos. Environ.*, 309, 10.1016/j.atmosenv.2023.119932, 2023.
- 635 He, Z., Wang, X., Ling, Z., Zhao, J., Guo, H., Shao, M., and Wang, Z.: Contributions of different anthropogenic volatile organic compound sources to ozone formation at a receptor site in the Pearl River Delta region and its policy implications, *Atmos. Chem. Phys.*, 19, 8801-8816, 10.5194/acp-19-8801-2019, 2019.
- Hofzumahaus, A., Rohrer, F., Lu, K., Bohn, B., Brauers, T., Chang, C.-C., Fuchs, H., Holland, F., Kita, K., Kondo, Y., Li, X., Lou, S., Shao, M., Zeng, L., Wahner, A., and Zhang, Y.: Amplified Trace Gas Removal in the Troposphere, *Science*, 324, 2009.
- 640 Hong, Z., Li, M., Wang, H., Xu, L., Hong, Y., Chen, J., Chen, J., Zhang, H., Zhang, Y., Wu, X., Hu, B., and Li, M.: Characteristics of atmospheric volatile organic compounds (VOCs) at a mountainous forest site and two urban sites in the southeast of China, *Sci Total Environ*, 657, 1491-1500, 10.1016/j.scitotenv.2018.12.132, 2019.
- 645 Huang, J. P., Fung, J. C. H., Lau, A. K. H., and Qin, Y.: Numerical simulation and process analysis of typhoon - related ozone episodes in Hong Kong, *Journal of Geophysical Research: Atmospheres*, 110, 10.1029/2004jd004914, 2005.



- Huang, W., Zhao, Q., Liu, Q., Chen, F., He, Z., Guo, H., and Ling, Z.: Assessment of atmospheric photochemical reactivity in the Yangtze River Delta using a photochemical box model, *Atmospheric Research*, 245, 10.1016/j.atmosres.2020.105088, 2020a.
- Huang, X. F., Wang, C., Zhu, B., Lin, L. L., and He, L. Y.: Exploration of sources of OVOCs in various atmospheres in southern China, *Environ Pollut*, 249, 831-842, 10.1016/j.envpol.2019.03.106, 2019.
- Huang, X. F., Zhang, B., Xia, S. Y., Han, Y., Wang, C., Yu, G. H., and Feng, N.: Sources of oxygenated volatile organic compounds (OVOCs) in urban atmospheres in North and South China, *Environ Pollut*, 261, 114152, 10.1016/j.envpol.2020.114152, 2020b.
- Huang, Y., Ling, Z. H., Lee, S. C., Ho, S. S. H., Cao, J. J., Blake, D. R., Cheng, Y., Lai, S. C., Ho, K. F., Gao, Y., Cui, L., and Louie, P. K. K.: Characterization of volatile organic compounds at a roadside environment in Hong Kong: An investigation of influences after air pollution control strategies, *Atmos. Environ.*, 122, 809-818, 10.1016/j.atmosenv.2015.09.036, 2015.
- Hui, L., Feng, X., Yuan, Q., Chen, Y., Xu, Y., Zheng, P., Lee, S., and Wang, Z.: Abundant oxygenated volatile organic compounds and their contribution to photochemical pollution in subtropical Hong Kong, *Environ Pollut*, 335, 122287, 10.1016/j.envpol.2023.122287, 2023.
- Karl, T., Striednig, M., Graus, M., Hammerle, A., and Wohlfahrt, G.: Urban flux measurements reveal a large pool of oxygenated volatile organic compound emissions, *Proc Natl Acad Sci U S A*, 115, 1186-1191, 10.1073/pnas.1714715115, 2018.
- Koss, A. R., Sekimoto, K., Gilman, J. B., Selimovic, V., Coggon, M. M., Zarzana, K. J., Yuan, B., Lerner, B. M., Brown, S. S., Jimenez, J. L., Krechmer, J., Roberts, J. M., Warneke, C., Yokelson, R. J., and de Gouw, J.: Non-methane organic gas emissions from biomass burning: identification, quantification, and emission factors from PTR-ToF during the FIREX 2016 laboratory experiment, *Atmos. Chem. Phys.*, 18, 3299-3319, 10.5194/acp-18-3299-2018, 2018.
- Li, B., Ho, S. S. H., Gong, S., Ni, J., Li, H., Han, L., Yang, Y., Qi, Y., and Zhao, D.: Characterization of VOCs and their related atmospheric processes in a central Chinese city during severe ozone pollution periods, *Atmos. Chem. Phys.*, 19, 617-638, 10.5194/acp-19-617-2019, 2019a.
- Li, H. Y., Canagaratna, M. R., Riva, M., Rantala, P., Zhang, Y. J., Thomas, S., Heikkinen, L., Flaud, P. M., Villenave, E., Perraudin, E., Worsnop, D., Kulmala, M., Ehn, M., and Bianchi, F.: Atmospheric organic vapors in two European pine forests measured by a Vocus PTR-TOF: insights into monoterpene and sesquiterpene oxidation processes, *Atmos. Chem. Phys.*, 21, 4123-4147, 10.5194/acp-21-4123-2021, 2021.
- Li, K., Jacob, D. J., Liao, H., Shen, L., Zhang, Q., and Bates, K. H.: Anthropogenic drivers of 2013-2017 trends in summer surface ozone in China, *Proc Natl Acad Sci U S A*, 116, 422-427, 10.1073/pnas.1812168116, 2019b.
- Li, K., Jacob, D. J., Shen, L., Lu, X., De Smedt, I., and Liao, H.: Increases in surface ozone pollution in China from 2013 to 2019: anthropogenic and meteorological influences, *Atmos. Chem. Phys.*, 20, 11423-11433, 10.5194/acp-20-11423-2020, 2020.
- Li, K., Chen, L., Ying, F., White, S. J., Jang, C., Wu, X., Gao, X., Hong, S., Shen, J., Azzi, M., and Cen, K.: Meteorological and chemical impacts on ozone formation: A case study in Hangzhou, China, *Atmospheric Research*, 196, 40-52, 10.1016/j.atmosres.2017.06.003, 2017.
- Li, L., Xie, S., Zeng, L., Wu, R., and Li, J.: Characteristics of volatile organic compounds and their role in ground-level ozone formation in the Beijing-Tianjin-Hebei region, China, *Atmos. Environ.*, 113, 247-254, 10.1016/j.atmosenv.2015.05.021, 2015.
- Li, X., Rohrer, F., Brauers, T., Hofzumahaus, A., Lu, K., Shao, M., Zhang, Y. H., and Wahner, A.: Modeling of HCHO and CHOCHO at a semi-rural site in southern China during the PRIDE-PRD2006 campaign, *Atmos. Chem. Phys.*, 14, 12291-12305, 10.5194/acp-14-12291-2014, 2014.



- Lin, H., Wang, M., Duan, Y., Fu, Q., Ji, W., Cui, H., Jin, D., Lin, Y., and Hu, K.: O₃ Sensitivity and Contributions of Different NMHC Sources in O₃ Formation at Urban and Suburban Sites in Shanghai, *Atmosphere-Basel*, 11, 10.3390/atmos11030295, 2020.
- 700 Liu, X., Lyu, X., Wang, Y., Jiang, F., and Guo, H.: Intercomparison of O₃ formation and radical chemistry in the past decade at a suburban site in Hong Kong, *Atmos. Chem. Phys.*, 19, 5127-5145, 10.5194/acp-19-5127-2019, 2019.
- 705 Liu, X., Wang, N., Lyu, X., Zeren, Y., Jiang, F., Wang, X., Zou, S., Ling, Z., and Guo, H.: Photochemistry of ozone pollution in autumn in Pearl River Estuary, South China, *Sci Total Environ*, 754, 141812, 10.1016/j.scitotenv.2020.141812, 2021.
- 710 Liu, Y., Qiu, P., Li, C., Li, X., Ma, W., Yin, S., Yu, Q., Li, J., and Liu, X.: Evolution and variations of atmospheric VOCs and O₃ photochemistry during a summer O₃ event in a county-level city, Southern China, *Atmos. Environ.*, 272, 10.1016/j.atmosenv.2022.118942, 2022.
- Lu, H., Cai, Q. Y., Wen, S., Chi, Y., Guo, S., Sheng, G., and Fu, J.: Seasonal and diurnal variations of carbonyl compounds in the urban atmosphere of Guangzhou, China, *Sci Total Environ*, 408, 3523-3529, 10.1016/j.scitotenv.2010.05.013, 2010.
- 715 Lyu, X., Guo, H., Zou, Q., Li, K., Xiong, E., Zhou, B., Guo, P., Jiang, F., and Tian, X.: Evidence for Reducing Volatile Organic Compounds to Improve Air Quality from Concurrent Observations and In Situ Simulations at 10 Stations in Eastern China, *Environ Sci Technol*, 56, 15356-15364, 10.1021/acs.est.2c04340, 2022.
- Ma, X., Tan, Z., Lu, K., Yang, X., Liu, Y., Li, S., Li, X., Chen, S., Novelli, A., Cho, C., Zeng, L., Wahner, A., and Zhang, Y.: Winter photochemistry in Beijing: Observation and model simulation of OH and HO(2) radicals at an urban site, *Sci Total Environ*, 685, 85-95, 10.1016/j.scitotenv.2019.05.329, 2019.
- 720 Mellouki, A., Bras, G. L., and Sidebottom, H.: Kinetics and Mechanisms of the Oxidation of Oxygenated Organic Compounds in the Gas Phase, *Chem Rev*, 103, 5077-5096, 2003.
- 725 Mills, G., Pleijel, H., Malley, C. S., Sinha, B., Cooper, O. R., Schultz, M. G., Neufeld, H. S., Simpson, D., Sharps, K., Feng, Z., Gerosa, G., Harmens, H., Kobayashi, K., Saxena, P., Paoletti, E., Sinha, V., and Xu, X.: Tropospheric Ozone Assessment Report: Present-day tropospheric ozone distribution and trends relevant to vegetation, *Elem Sci Anth*, 6, 47, 10.1525/journal.elementa.302, 2018.
- 730 Mo, Z., Shao, M., and Lu, S.: Compilation of a source profile database for hydrocarbon and OVOC emissions in China, *Atmos. Environ.*, 143, 209-217, 10.1016/j.atmosenv.2016.08.025, 2016.
- Rohrer, F., Lu, K., Hofzumahaus, A., Bohn, B., Brauers, T., Chang, C.-C., Fuchs, H., Häseler, R., Holland, F., Hu, M., Kita, K., Kondo, Y., Li, X., Lou, S., Oebel, A., Shao, M., Zeng, L., Zhu, T., Zhang, Y., and Wahner, A.: Maximum efficiency in the hydroxyl-radical-based self-cleansing of the troposphere, *Nature Geoscience*, 7, 559-563, 10.1038/ngeo2199, 2014.
- 735 Shen, H., Liu, Y., Zhao, M., Li, J., Zhang, Y., Yang, J., Jiang, Y., Chen, T., Chen, M., Huang, X., Li, C., Guo, D., Sun, X., Xue, L., and Wang, W.: Significance of carbonyl compounds to photochemical ozone formation in a coastal city (Shantou) in eastern China, *Sci Total Environ*, 764, 144031, 10.1016/j.scitotenv.2020.144031, 2021.
- 740 Sun, H., Gu, D., Feng, X., Wang, Z., Cao, X., Sun, M., Ning, Z., Zheng, P., Mai, Y., Xu, Z., Chan, W. M., Li, X., Zhang, W., Lee, H. W., Leung, K. F., Yu, J. Z., Lee, E., Louie, P. K. K., and Leung, K.: Cruise observation of ambient volatile organic compounds over Hong Kong coastal water, *Atmos. Environ.*, 323, 10.1016/j.atmosenv.2024.120387, 2024.
- 745 Tan, Z., Lu, K., Jiang, M., Su, R., Dong, H., Zeng, L., Xie, S., Tan, Q., and Zhang, Y.: Exploring ozone pollution in Chengdu, southwestern China: A case study from radical chemistry to O(3)-VOC-NO(x) sensitivity, *Sci Total Environ*, 636, 775-786, 10.1016/j.scitotenv.2018.04.286, 2018.



- Tan, Z., Lu, K., Jiang, M., Su, R., Wang, H., Lou, S., Fu, Q., Zhai, C., Tan, Q., Yue, D., Chen, D., Wang, Z., Xie, S., Zeng, L., and Zhang, Y.: Daytime atmospheric oxidation capacity in four Chinese megacities during the photochemically polluted season: a case study based on box model simulation, *Atmos. Chem. Phys.*, 19, 3493-3513, 10.5194/acp-19-3493-2019, 2019a.
- Tan, Z., Lu, K., Hofzumahaus, A., Fuchs, H., Bohn, B., Holland, F., Liu, Y., Rohrer, F., Shao, M., Sun, K., Wu, Y., Zeng, L., Zhang, Y., Zou, Q., Kiendler-Scharr, A., Wahner, A., and Zhang, Y.: Experimental budgets of OH, HO₂, and RO₂ radicals and implications for ozone formation in the Pearl River Delta in China 2014, *Atmos. Chem. Phys.*, 19, 7129-7150, 10.5194/acp-19-7129-2019, 2019b.
- Wang, H., Lyu, X., Guo, H., Wang, Y., Zou, S., Ling, Z., Wang, X., Jiang, F., Zeren, Y., Pan, W., Huang, X., and Shen, J.: Ozone pollution around a coastal region of South China Sea: interaction between marine and continental air, *Atmos. Chem. Phys.*, 18, 4277-4295, 10.5194/acp-18-4277-2018, 2018a.
- Wang, N., Guo, H., Jiang, F., Ling, Z. H., and Wang, T.: Simulation of ozone formation at different elevations in mountainous area of Hong Kong using WRF-CMAQ model, *Sci Total Environ.*, 505, 939-951, 10.1016/j.scitotenv.2014.10.070, 2015.
- Wang, R., Wang, L., Yang, Y., Zhan, J., Ji, D., Hu, B., Ling, Z., Xue, M., Zhao, S., Yao, D., Liu, Y., and Wang, Y.: Comparative analysis for the impacts of VOC subgroups and atmospheric oxidation capacity on O(3) based on different observation-based methods at a suburban site in the North China Plain, *Environ Res.*, 248, 118250, 10.1016/j.envres.2024.118250, 2024.
- Wang, W., Yuan, B., Peng, Y., Su, H., Cheng, Y., Yang, S., Wu, C., Qi, J., Bao, F., Huangfu, Y., Wang, C., Ye, C., Wang, Z., Wang, B., Wang, X., Song, W., Hu, W., Cheng, P., Zhu, M., Zheng, J., and Shao, M.: Direct observations indicate photodegradable oxygenated volatile organic compounds (OVOCs) as larger contributors to radicals and ozone production in the atmosphere, *Atmos. Chem. Phys.*, 22, 4117-4128, 10.5194/acp-22-4117-2022, 2022a.
- Wang, X., Yin, S., Zhang, R., Yuan, M., and Ying, Q.: Assessment of summertime O(3) formation and the O(3)-NO(X)-VOC sensitivity in Zhengzhou, China using an observation-based model, *Sci Total Environ.*, 813, 152449, 10.1016/j.scitotenv.2021.152449, 2022b.
- Wang, Y., Guo, H., Zou, S., Lyu, X., Ling, Z., Cheng, H., and Zeren, Y.: Surface O(3) photochemistry over the South China Sea: Application of a near-explicit chemical mechanism box model, *Environ Pollut.*, 234, 155-166, 10.1016/j.envpol.2017.11.001, 2018b.
- Wang, Y., Wang, H., Guo, H., Lyu, X., Cheng, H., Ling, Z., Louie, P. K. K., Simpson, I. J., Meinardi, S., and Blake, D. R.: Long-term O₃-precursor relationships in Hong Kong: field observation and model simulation, *Atmos. Chem. Phys.*, 17, 10919-10935, 10.5194/acp-17-10919-2017, 2017.
- Wolfe, G. M., Marvin, M. R., Roberts, S. J., Travis, K. R., and Liao, J.: The Framework for 0-D Atmospheric Modeling (F0AM) v3.1, *Geosci Model Dev.*, 9, 3309-3319, 10.5194/gmd-9-3309-2016, 2016.
- Wu, C., Wang, C., Wang, S., Wang, W., Yuan, B., Qi, J., Wang, B., Wang, H., Wang, C., Song, W., Wang, X., Hu, W., Lou, S., Ye, C., Peng, Y., Wang, Z., Huangfu, Y., Xie, Y., Zhu, M., Zheng, J., Wang, X., Jiang, B., Zhang, Z., and Shao, M.: Measurement report: Important contributions of oxygenated compounds to emissions and chemistry of volatile organic compounds in urban air, *Atmos. Chem. Phys.*, 20, 14769-14785, 10.5194/acp-20-14769-2020, 2020.
- Xu, C., He, X., Sun, S., Bo, Y., Cui, Z., Zhang, Z., and Dong, H.: Sensitivity of Ozone Formation in Summer in Jinan Using Observation-Based Model, *Atmosphere-Basel*, 13, 10.3390/atmos13122024, 2022.
- Xue, L., Gu, R., Wang, T., Wang, X., Saunders, S., Blake, D., Louie, P. K. K., Luk, C. W. Y., Simpson, I., Xu, Z., Wang, Z., Gao, Y., Lee, S., Mellouki, A., and Wang, W.: Oxidative



- capacity and radical chemistry in the polluted atmosphere of Hong Kong and Pearl River Delta region: analysis of a severe photochemical smog episode, *Atmos. Chem. Phys.*, 16, 9891-9903, 10.5194/acp-16-9891-2016, 2016.
- 800 Yang, X., Feng, X., Chen, Y., Zheng, P., Hui, L., Chen, Y., Yu, J. Z., and Wang, Z.: Development of an enhanced method for atmospheric carbonyls and characterizing their roles in photochemistry in subtropical Hong Kong, *Sci Total Environ*, 165135, 10.1016/j.scitotenv.2023.165135, 2023.
- 805 Yang, X., Xue, L., Wang, T., Wang, X., Gao, J., Lee, S., Blake, D. R., Chai, F., and Wang, W.: Observations and Explicit Modeling of Summertime Carbonyl Formation in Beijing: Identification of Key Precursor Species and Their Impact on Atmospheric Oxidation Chemistry, *Journal of Geophysical Research: Atmospheres*, 123, 1426-1440, 10.1002/2017jd027403, 2018.
- 810 Yang, X., Xue, L., Yao, L., Li, Q., Wen, L., Zhu, Y., Chen, T., Wang, X., Yang, L., Wang, T., Lee, S., Chen, J., and Wang, W.: Carbonyl compounds at Mount Tai in the North China Plain: Characteristics, sources, and effects on ozone formation, *Atmospheric Research*, 196, 53-61, 10.1016/j.atmosres.2017.06.005, 2017.
- 815 Yang, Y., Ji, D., Sun, J., Wang, Y., Yao, D., Zhao, S., Yu, X., Zeng, L., Zhang, R., Zhang, H., Wang, Y., and Wang, Y.: Ambient volatile organic compounds in a suburban site between Beijing and Tianjin: Concentration levels, source apportionment and health risk assessment, *Sci Total Environ*, 695, 133889, 10.1016/j.scitotenv.2019.133889, 2019.
- Yu, D., Tan, Z., Lu, K., Ma, X., Li, X., Chen, S., Zhu, B., Lin, L., Li, Y., Qiu, P., Yang, X., Liu, Y., Wang, H., He, L., Huang, X., and Zhang, Y.: An explicit study of local ozone budget and NO_x-VOCs sensitivity in Shenzhen China, *Atmos. Environ.*, 224, 10.1016/j.atmosenv.2020.117304, 2020.
- 820 Yuan, B., Koss, A. R., Warneke, C., Coggon, M., Sekimoto, K., and de Gouw, J. A.: Proton-Transfer-Reaction Mass Spectrometry: Applications in Atmospheric Sciences, *Chem Rev*, 117, 13187-13229, 10.1021/acs.chemrev.7b00325, 2017.
- 825 Yue, X. and Unger, N.: Ozone vegetation damage effects on gross primary productivity in the United States, *Atmos. Chem. Phys.*, 14, 9137-9153, 10.5194/acp-14-9137-2014, 2014.
- Zhang, J., Wang, T., Chameides, W. L., Cardelino, C., Kwok, J., Blake, D. R., Ding, A., and So, K. L.: Ozone production and hydrocarbon reactivity in Hong Kong, Southern China, *Atmos. Chem. Phys.*, 7, 557-573, 2007.
- 830 Zhang, Y., Dai, W., Li, J., Ho, S. S. H., Li, L., Shen, M., Wang, Q., and Cao, J.: Comprehensive observations of carbonyls of Mt. Hua in Central China: Vertical distribution and effects on ozone formation, *Sci Total Environ*, 907, 167983, 10.1016/j.scitotenv.2023.167983, 2024.
- Zhang, Y. H., Su, H., Zhong, L. J., Cheng, Y. F., Zeng, L. M., Wang, X. S., Xiang, Y. R., Wang, J. L., Gao, D. F., and Shao, M.: Regional ozone pollution and observation-based approach for analyzing ozone-precursor relationship during the PRIDE-PRD2004 campaign, *Atmos. Environ.*, 42, 6203-6218, 10.1016/j.atmosenv.2008.05.002, 2008.
- 835 Zhang, Z., Man, H., Duan, F., Lv, Z., Zheng, S., Zhao, J., Huang, F., Luo, Z., He, K., and Liu, H.: Evaluation of the VOC pollution pattern and emission characteristics during the Beijing resurgence of COVID-19 in summer 2020 based on the measurement of PTR-ToF-MS, *Environ Res Lett*, 17, 10.1088/1748-9326/ac3e99, 2022.
- 840 Zhao, M., Zhang, Y., Pei, C., Chen, T., Mu, J., Liu, Y., Wang, Y., Wang, W., and Xue, L.: Worsening ozone air pollution with reduced NO_x and VOCs in the Pearl River Delta region in autumn 2019: Implications for national control policy in China, *J Environ Manage*, 324, 116327, 10.1016/j.jenvman.2022.116327, 2022.
- 845 Zhao, Y., Chen, L., Li, K., Han, L., Zhang, X., Wu, X., Gao, X., Azzi, M., and Cen, K.: Atmospheric ozone chemistry and control strategies in Hangzhou, China: Application of a 0-D box model, *Atmospheric Research*, 246, 10.1016/j.atmosres.2020.105109, 2020.



850 Zhou, X., Li, Z. Q., Zhang, T. J., Wang, F., Wang, F. T., Tao, Y., Zhang, X., Wang, F. L., and
Huang, J.: Volatile organic compounds in a typical petrochemical industrialized valley city of
northwest China based on high-resolution PTR-MS measurements: Characterization, sources
and chemical effects, *Sci. Total Environ.*, 671, 883-896, 10.1016/j.scitotenv.2019.03.283, 2019.